

## Contact-inhibited chemotactic motility: Role in *de novo* and sprouting blood vessel growth

Roeland M. H. Merks,<sup>1,\*</sup> Erica D. Perryn,<sup>2,†</sup> and James A. Glazier<sup>1</sup>

<sup>1</sup>*The Biocomplexity Institute and Department of Physics, Indiana University Bloomington,  
Swain Hall West 159, 727 E 3rd Street, Bloomington, IN 47405, USA*

<sup>2</sup>*The University of Kansas Medical Center, Dept. Anatomy and Cell Biology,  
1008 Wahl Hall West, Mail Stop 3038, 3901 Rainbow Boulevard, Kansas City, KS 66160, USA*

(Dated: February 9, 2020)

Blood vessels form either when dispersed endothelial cells (the cells lining the inner walls of fully formed blood vessels) organize into a vessel networks (*vasculogenesis*), or by sprouting or splitting of existing blood vessels (*angiogenesis*). Although these mechanisms are closely related biologically, modelers traditionally consider them separately. No current model explains both phenomena with a single biophysical mechanism. In addition, many computational models describe sprouting at the level of the blood vessel, ignoring how cell behavior drives branch splitting sprouting. We present a computational model based on plausible behavior of endothelial cells, that reproduces aspects of both *de novo* and sprouting blood vessel growth and discuss the branching instability responsible for our results. The branching mechanism, driven by contact-inhibition of chemotaxis, is both a generic developmental mechanism and an interesting example of an unusual type of patterning instability.

PACS numbers: 87.18.Hf; 87.18.Bb; 87.17.Jj; 89.75.Kd; 61.43.Hv

Blood vessel development is essential for myriad biological phenomena in healthy and diseased individuals, including wound healing and tumor growth [1]. Blood vessels form either *de novo*, when dispersed *endothelial cells* (*ECs*; the cells lining the inner walls of fully formed blood vessels) organize into a vascular network (*vasculogenesis*), or by sprouting or splitting of existing blood vessels (*angiogenesis*). Many computer models exist to explain and describe either *de novo* [2, 3, 4, 5, 6] or sprouting blood vessel growth [7, 8, 9]. However, the same genetic machinery regulates both mechanisms, which are closely related [10], so a plausible mechanism must explain both.

Blood vessel growth requires the cell-adhesion molecule *vascular-endothelial-cadherin* (*VE-cadherin*) [11], which clusters at endothelial cell interfaces and modulates vascular-endothelial growth-factor-A's (*VEGF-A*) effect on ECs; *VEGF-A* is a potent growth-factor, which stimulates blood vessel sprouting. In the presence of *VE-cadherin* binding, *VEGF-A* inhibits *EC* motility and proliferation. In the absence of *VE-cadherin* binding, *VEGF-A* activates pathways related to actin polymerization and the cell cycle, triggering cell motility and proliferation in sub-confluent monolayers [12]. Thus, we hypothesize that *VE-cadherin* binding at cell-cell interfaces represses the formation of chemotactic surface projections (*filopodia*), while filopodia form normally at unbound parts of the cell surface.

In this letter we show that such contact-inhibition of chemotactic projections, in combination with secretion of a diffusive, rapidly decaying chemoattractant by the ECs may drive a developmental mechanism which can reproduce both *de novo* and sprouting blood vessel growth. We model endothelial cells that a) secrete a chemoattractant; b) preferentially extend filopodia up gradients of the chemoattractant, unless c) contact inhi-

bition prevents chemotactic filopodium extension. The endothelial cells are polar: cell-cell binding suppresses the extension of chemotactic filopodia, while the unbound cell surfaces in contact with the extracellular matrix (*ECM*; the non-living mixture of proteins, growth-factors and carbohydrates surrounding the cells) continue to extend filopodia towards the chemoattractant [13]. In our current model, we further assume that *VEGF-A* is not limiting and distributes uniformly over the *ECM*, as in the widely-used human-umbilical-cord vascular-endothelial cell (*HUVEC*) cultures [3] or in murine or avian yolk sacs [11].

We model endothelial cell behavior at a mesoscopic level using the Cellular Potts Model [14] (*CPM*), a Monte-Carlo approach in which we bias membrane fluctuations and extensions of filopodia according to the concentration of chemoattractant. We describe chemoattractant diffusion macroscopically, using a continuum approximation. An energy-minimization philosophy, a set of constraints and auxiliary conditions determine how the cells move. Intercellular junctions and cell junctions to the *ECM* determine an adhesive (or binding) energy. Cells move to promote stronger rather than weaker bonds and shorter rather than longer cell boundaries. An energy constraint regulates cell volume or surface area. Because we compare our simulations to yolk sac cultures, where vascular patterns are essentially monolayers, we can use a two-dimensional *CPM*.

The *CPM* represents biological cells as patches of identical lattice spins  $\sigma(\vec{x})$  on a square lattice, where each spin identifies, or “labels” a single biological cell. Connections between neighboring lattice sites of unlike spin  $\sigma(\vec{x}) \neq \sigma(\vec{x}')$  represent membrane bonds, where the *bond energy* is  $J_{\sigma_{\vec{x}}, \sigma_{\vec{x}'}}$ , assuming that the types and number of adhesive cell-surface proteins determine  $J$ . An energy

penalty increasing with the cell's deviation from a designated target volume  $A_\sigma$  imposes a *volume constraint* on the biological cells. We define the pattern Hamiltonian:

$$H = \sum_{\vec{x}, \vec{x}'} J_{\sigma_{\vec{x}}, \sigma_{\vec{x}'}} (1 - \delta_{\sigma_{\vec{x}}, \sigma_{\vec{x}'}}) + \lambda \sum_{\sigma} (a_\sigma - A_\sigma)^2, \quad (1)$$

where  $\lambda$  represents a cell's resistance to compression, and the Kronecker delta is  $\delta_{x,y} = \{1, x = y; 0, x \neq y\}$ . Each lattice site represents an area of  $2 \mu m \times 2 \mu m$ . We assume that cells do not divide or grow during patterning, with  $A_\sigma = 50$  lattice sites and  $\lambda = 25$  for all cells. The cells reside in an ECM which is a generalized CPM cell without a volume constraint and with  $\sigma = 0$ . We use a bond energy  $J_{cc} = 40$  between the endothelial cells, and  $J_{cM} = 20$  between the endothelial cells and the ECM; for these settings the cells do not adhere without chemotaxis. We define a special, high *cell-border energy*  $J_{cB} = 100$  to prevent cells from adhering to the lattice boundaries.

To mimic cytoskeletally driven membrane fluctuations, we randomly choose a lattice site,  $\vec{x}$ , and attempt to copy its spin  $\sigma_{\vec{x}}$  into a randomly chosen neighboring lattice site  $\vec{x}'$ . For better isotropy we use the twenty, first to fourth nearest neighbors [15]. During a *Monte Carlo Step (MCS)* we carry out  $n$  copy attempts, with  $n$  the number of sites in the lattice. We set the time per MCS at 30 s.

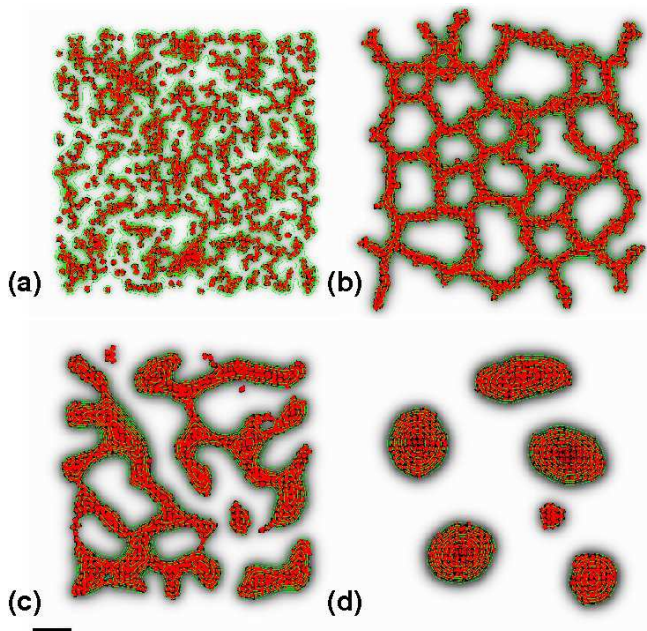


FIG. 1: Vascular network formation in a simulation initiated with 1000 scattered endothelial cells: (a) 10 MCS; (b) 10000 MCS; (c,d) Disrupted *de novo* blood vessel growth in a simulation without contact-inhibition of chemotaxis ( $\chi_{cc}/\chi_{cM} = 1$ ). (c) 1000 MCS; (d) 10000 MCS. Scale bar: 50 sites ( $\approx 100 \mu m$ ). Contour lines (green) indicate ten chemoattractant levels relative to the maximum concentration in the simulation. Greyscale indicates absolute concentration on a logarithmic scale.

We calculate how much the Hamiltonian would change if we performed the copy, and accept the attempt with probability,  $P(\Delta H) = \{e^{-\frac{\Delta H}{T}}, \Delta H \geq 0; 1, \Delta H < 0\}$ . All our simulations use a Boltzmann temperature  $T = 50$ .

In analogy to a previous PDE approach of *de novo* blood vessel growth [3, 4], every site within the CPM cells secretes the chemoattractant, which only decays in the ECM:

$$\frac{\partial c}{\partial t} = \alpha \delta_{\sigma_{\vec{x}}, 0} - (1 - \delta_{\sigma_{\vec{x}}, 0}) \epsilon c + D \nabla^2 c, \quad (2)$$

where  $\delta_{\sigma_{\vec{x}}, 0} = 1$  inside the cells.  $\alpha = 10^{-3} s^{-1}$  is the rate at which the cells release chemoattractant,  $\epsilon = \alpha$  is the decay rate of the chemoattractant, which diffuses slowly at  $D = 10^{-13} m^2 s^{-1}$ . These parameter values produce steeper gradients than VEGF-A, the chemoattractant suggested by Gamba *et al.* [3]. However, VEGF-A is an unlikely candidate for the chemoattractant, since it is ubiquitously available in the ECM and it is most likely not produced by endothelial cells (see discussion and candidate chemoattractants in [16]). We solve this PDE numerically using a finite-difference scheme on a lattice that matches the CPM lattice, using 15 diffusion steps per MCS with  $\Delta t = 2$  s. For these parameters, the chemoattractant diffuses more rapidly than the cells, enabling us to ignore advection as the cells push the ECM.

We implement preferential extension of filopodia in the direction of chemoattractant gradients [13] by allowing for an extra energy drop at the time of copying [17],  $\Delta H_{\text{chemotaxis}} = -\mu(c(\vec{x}') - c(\vec{x}))$ , where  $\vec{x}'$  is the neighbor into which site  $\vec{x}$  copies its spin, and  $\mu = \chi_{cM}$

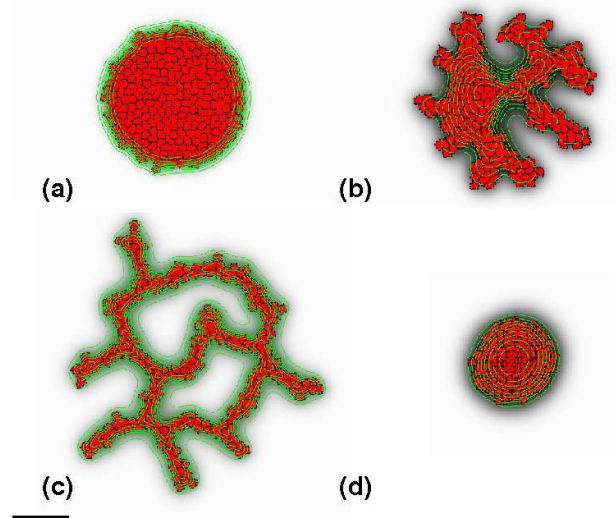


FIG. 2: Sprouting instability in a simulation initiated with a clump of endothelial cells: (a) 10 MCS; (b) 1000 MCS; (c) 10000 MCS; (d) disrupted sprouting blood vessel growth in a simulation without contact-inhibition of chemotaxis ( $\chi_{cc}/\chi_{cM} = 1$ ); 10000 MCS. Scale bar: 50 sites ( $\approx 100 \mu m$ ).

and  $\mu = \chi_{cc}$  at cell-ECM and cell-cell interfaces respectively. We use a value of  $\chi_{cM} = 500$ , while setting  $\chi_{cc} = 0$  ensures that chemotactic extensions occur only at cell-matrix interfaces, reflecting VE-cadherin’s suppression of filopodia. Experimental evidence indicates that HL60 cells do not accelerate in chemoattractant gradients, but instead assume a flow-dependent, constant velocity [18]. In the CPM, cells also obey this overdamped force-velocity response (i.e. the velocity is proportional to the chemical gradient; see e.g. [16]), unlike previous models that assumed cells accelerate in chemoattractant gradients [3, 4]. Hence without contact-inhibition of chemotaxis ( $\chi_{cM} = \chi_{cc}$ ), our model assumptions reduce to the classic Keller-Segel equations of chemotactic aggregation [19], in which case our model forms isolated island patterns as expected (Fig. 1(c,d)); see also [4]).

Fig. 1(a-b) shows typical simulated *de novo* blood-vessel growth. We randomly distributed 1000 endothelial cells over an area of  $333 \times 333$  lattice sites, which we positioned in a larger lattice of  $500 \times 500$  to minimize boundary effects. The endothelial cells assembled into a structure resembling a capillary plexus: *chords* of cells enclose *lacunae* which reach a roughly uniform size over time. Smaller lacunae shrink and disappear, while the subdivision of larger lacunae resembles vessel sprouting [25] as e.g. in the quail yolk sac [20]. In Fig. 1(c-d) we disrupt contact-inhibition of chemotaxis by setting  $\chi_{cc} = \chi_{cM}$ , and allowing for chemotactic filopodia both at cell-ECM and at cell-cell interfaces. A vascular network no longer forms and the cells aggregate into small “islands.”

In Fig. 2 we initiate the simulation with a mass of endothelial cells instead, keeping all other parameters the same. This would represent the blood vessel’s surface after degradation of the extracellular matrix. After an initial “roughening,” the blob’s surface digitates into a structure reminiscent of a vascular network (Fig. 2 (c)), the first structure to develop both in *de novo* and in sprouting blood vessel growth [20]. Thus our simulation suggests that a single process at the level of the EC may drive both sprouting and *de novo*, *in vitro* blood vessel growth. The sprouting instability also requires contact-inhibition of chemotaxis, without it the cluster remains rounded and contracts (Fig. 2(d)).

We compared our model predictions to *in vitro* cultures of mouse allantois explants [21, 22][26]. The endothelial cells (fluorescently labeled in red) organize into polygonal patterns, as in our simulations (Fig. 3(a-c)). After experimentally blocking VE-cadherin receptors with anti-VE-cadherin antibodies, the cells form isolated vascular islands (Fig. 3(d-f) as in the simulations, and in yolk sacs of VE-cadherin  $-/-$  mice [11]. We hypothesize anti-VE-cadherin’s blockage of VE-cadherin prevents contact-inhibition of chemotactic motility, sensitizing the endothelial cells to the chemoattractant at cell-cell interfaces. After anti-VE-cadherin treatment ECs assume a

more rounded shape; thus the experiments currently cannot distinguish between contact-inhibited chemotaxis or the cell-shape dependent mechanisms [16]. Future studies, including time-lapse microscopy [23] allowing for dynamic comparison of cell cultures and simulations (see e.g. [16]) will help us distinguish these possibilities.

Our simulations suggest how contact-inhibited chemotactic migration could drive blood vessel sprouting. At equilibrium, the chemoattractant has a Gaussian-like profile, which levels off towards the cluster’s center. Thus, without contact-inhibition of chemotaxis all cells, also those in the cluster’s interior, try to move towards the center, compressing interior cells (Fig. 2d) that resist displacement. Contact-inhibition of chemotaxis leaves the interior cells insensitive to the chemoattractant, which are easily pushed aside by ingressing surface cells. Hence we may consider the cluster as a contracting shell undergoing a buckling-type instability.

To explore this idea, we varied the chemotactic response at cell-cell interfaces,  $\chi_{cc}$ . We looked for sprouting in clusters of 128 cells placed in a  $200 \times 200$  lattice, keeping all other parameters unchanged. We measured the clusters’ compactness after 10000 MCS, as  $C = A_{\text{cluster}}/A_{\text{hull}}$ , the ratio between a cluster’s area and its convex hull, as a function of the chemotactic response at cell-cell interfaces relative to chemotaxis at cell-ECM interfaces ( $\chi_{cc}/\chi_{cM}$ ). We found a phase transition at  $\chi_{cc}/\chi_{cM} \approx 0.5$  separating sprouting from non-sprouting clusters (Fig. 4). This suggests that the buckling-like sprouting instability only occurs when the core of the cluster is sufficiently fluid. We are now mathematically characterizing this instability.

Continuum approaches explain *de novo* blood vessel growth by assuming that ECs actively move along VEGF-A gradients [3, 4], or that ECs exert stresses on the ECM [2], thus pulling the surrounding ECs towards them or providing cues for active migration (*haptotaxis*)

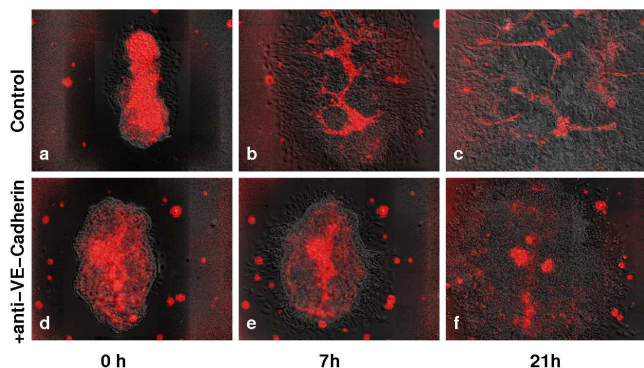


FIG. 3: Anti-VE-cadherin antibody inhibits *de novo* blood vessel growth in allantois cultures. Endothelial cells fluorescently labeled in red with endothelium specific CD34-Cy3 antibody. DIC/fluorescent image overlays. (a-c) control, (d-f) anti-VE-cadherin treated cell cultures.

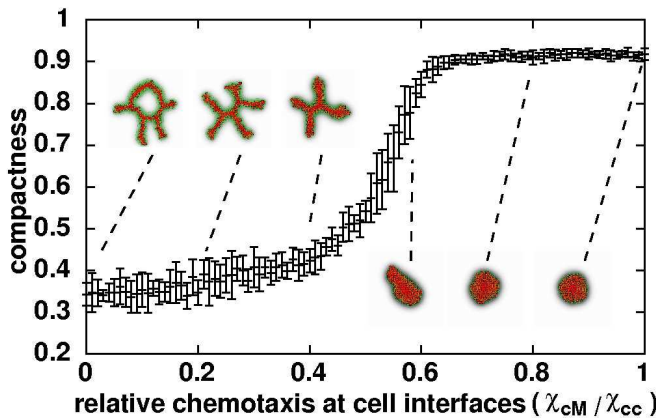


FIG. 4: Compactness ( $C = A_{\text{cluster}}/A_{\text{hull}}$ ) of 128-cell clusters after 10000 MCS ( $\approx 80 h$ ) as a function of the relative chemotactic response at cell-cell interfaces. Error bars: standard deviation over ten simulations.

[5], or both [6]. Because these models assume the ECs exert radially symmetric stresses on the ECM, the generic mechanism behind both approaches is similar and involves movement of ECs up either chemical or mechanical gradients around cell clusters. Consequently, the patterning mechanism we described here likely holds if we assumed mechanical or haptotactic, instead of chemical gradients.

Previous work has treated *de novo* and sprouting blood vessel growth as separate phenomena. Here we have shown that a single set of endothelial cell behaviors can explain aspects of both. Many models of sprouting blood-vessel growth explicitly introduce blood-vessel-level phenomenology through a high-level rule for branching [7, 8, 9], which experiments do not support. Our model does not need such vessel-level phenomenology; the observed branching instability and pattern formation require only experimentally-observed phenomenology at the level of individual ECs. Our current work focused on instability of EC clusters, ignoring the directed blood-vessel sprouting along morphogen gradients that these models consider. Future work will include directed sprouting, *e.g.* by including additional EC chemoattractants or chemorepellants. Also, we have ignored here the possible roles of cell-adhesion, saturation of chemotactic receptors [24], cell elongation [16] and absolute chemotactic response ( $\chi_{cM}$ ); we will present full studies of these parameters elsewhere.

We gratefully acknowledge discussions with Stuart Newman, András Czirók, Charles Little, and Abbas Shirini. RM developed parts of the simulation software during work with Paulien Hogeweg at Utrecht University, The Netherlands. This work received support from NSF grants IBN-0083653 (JAG), NASA Glenn Research Center NAG 2-1619 (JAG), a Pervasive Technologies Laboratories Fellowship (Indiana University Bloomington), an IBM Innovation Institute Award (JAG), the IU Biocomplexity Institute (RM), the IU AVIDD program (JAG;

RM) and American Heart Association predoctoral fellowship 0410084Z (EDP).

\* Electronic address: post@roelandmerks.nl; Present address: Dept. Plant Systems Biology, Flanders Interuniversity Institute of Biotechnology/UGhent, Technologiepark 927, B-9052 Ghent, Belgium

† Electronic address: eperryn@kumc.edu

- [1] P. Carmeliet and R. K. Jain, *Nature* **407**, 249 (2000).
- [2] D. Manoussaki, S. R. Lubkin, R. B. Vernon, and J. D. Murray, *Acta Biotheor.* **44**, 271 (1996).
- [3] A. Gamba, D. Ambrosi, A. Coniglio, A. De Candia, S. Di Talia, E. Giraudo, G. Serini, L. Preziosi, and F. Busiolino, *Phys. Rev. Lett.* **90**, 118101 (2003).
- [4] D. Ambrosi, A. Gamba, and G. Serini, *B. Math. Biol.* **66**, 1851 (2004).
- [5] P. Namy, J. Ohayon, and P. Tracqui, *J. Theor. Biol.* **227**, 103 (2004).
- [6] A. Tosin, D. Ambrosi, and L. Preziosi, *Bull. Math. Biol.* pp. doi:10.1007/s11538-006-9071-2 (in press).
- [7] A. R. A. Anderson and M. A. J. Chaplain, *B. Math. Biol.* **60**, 857 (1998).
- [8] S. Tong and F. Yuan, *Microvasc. Res.* **61**, 14 (2001).
- [9] S. Y. Sun, M. F. Wheeler, M. Obeyesekere, and C. W. Patrick, *B. Math. Biol.* **67**, 313 (2005).
- [10] P. Carmeliet, *Nat. Med.* **6**, 389 (2000).
- [11] S. Gory-Fauré, M.-H. Prandini, H. Pointu, V. Roullot, I. Pignot-Paintrand, M. Vernet, and P. Huber, *Development* **126**, 2093 (1999).
- [12] E. Dejana, *Nat. Rev. Mol. Cell Bio.* **5**, 261 (2004).
- [13] H. Gerhardt, M. Golding, M. Fruttiger, C. Ruhrberg, A. Lundkvist, A. Abramsson, M. Jeltsch, C. Mitchell, K. Alitalo, D. Shima, et al., *J. Cell Biol.* **161**, 1163 (2003).
- [14] J. A. Glazier and F. Graner, *Phys. Rev. E* **47**, 2128 (1993).
- [15] E. A. Holm, J. A. Glazier, D. J. Srolovitz, and G. S. Grest, *Phys. Rev. A* **43**, 2662 (1991).
- [16] R. M. H. Merks, S. V. Brodsky, M. S. Goligorsky, S. A. Newman, and J. A. Glazier, *Dev. Biol.* **289**, 44 (2006).
- [17] N. J. Savill and P. Hogeweg, *J. Theor. Biol.* **184**, 229 (1997).
- [18] G. M. Walker, J. Sai, A. Richmond, M. Stremmler, C. Y. Chung, and J. P. Wikswo, *Lab Chip* **5**, 611 (2005).
- [19] E. F. Keller and L. A. Segel, *J. Theor. Biol.* **26**, 399 (1970).
- [20] W. Riseau, *Nature* **386**, 671 (1997).
- [21] C. J. Drake and P. A. Fleming, *Blood* **95**, 1671 (2000).
- [22] K. M. Downs, S. Gifford, M. Blahnik, and R. L. Gardner, *Development* **125**, 4507 (1998).
- [23] A. Czirok, P. A. Rupp, B. J. Rongish, and C. D. Little, *Journal of Microscopy* **206**, 209 (2002).
- [24] R. M. H. Merks, S. A. Newman, and J. A. Glazier, *Lect. Notes Comput. Sc.* **3305**, 425 (2004).
- [25] See EPAPS Document No. [number] (temporarily at <http://www.psb.ugent.be/~romer/PRL/>) for movies of the simulations in Figs. 1-2. For more information on EPAPS, see <http://www.aip.org/pubservs/epaps.html>.
- [26] See EPAPS Document No. [number] for Materials and Methods.